Supporting Information for "Climate sensitivity increases under higher CO_2 levels due to feedback temperature dependence"

Jonah Bloch-Johnson[1], Maria Rugenstein[2], Martin B. Stolpe, Tim Rohrschneider[2], Yiyu Zheng[2], and Jonathan Gregory[1,3]

[1]NCAS, University of Reading

[2]Max-Planck-Institute for Meteorology

[3]Met Office Hadley Centre

Contents of this file

1. General information (Table S1 and Text S1)

Table S1 gives a glossary of all terms used in the paper. Text S1 explains how bootstrapped uncertainties were calculated.

2. Equilibrium warming (Figure S1 to S2 and Table S2)

Fig. S1 shows plots of N vs. T for all simulations used in the paper. Table S1 shows the number of years used in estimates of equilibrium warming that use more than 150 years. Fig. S2 provides a similar plot to Fig. 1a with an alternative definition of ECS.

3. Radiative forcing (Figures S3 to S4)

Fig. S3 illustrates that alternative methods for estimating the change in forcing per doubling with CO_2 concentration do not affect our conclusion that forcing is insufficient to explain the sensitivity increase. Fig. S4 provides estimates of the nonlinearity of the forcing for each model.

4. Radiative feedback (Figure S5, Tables S3 to S4, and Text S2)

Table S2 shows estimates of feedback CO_2 dependence. Text S2 provides more details of these estimates. Fig. S5 shows how minimal and maximal values based on these estimates affect Fig. 2, as well using the first twenty years instead of the first ten years to estimate radiative forcing, using direct estimates of forcing instead of a quadratic fit, and using fewer years to estimate equilibrium warming. Table S3 shows models with abrupt4xCO_2 estimates greater than 9K.

5. Comparing nonlinear terms (Text S3, Figure S6 to S7)

Text S3 gives details of estimating the flux components of the three nonlinear terms discussed in this paper. Fig. S6 shows the flux components of the preindustrial feedback and feedback temperature dependence, while Fig. S7 shows the flux components of the nonlinear forcing and the feedback CO_2 dependence.

1. General information

Table S1. Symbols used in the manuscript.

	Name	Units	Definition	Under the linear assumption (Eq. 6)	Under the quadratic assumption (Eq. 9)	Notes
pCO_2	CO_2 concentration	ppm	global-mean tropospheric CO_2 concentration			
$pCO_{2,pi}$	preindustrial CO_2 concentration	ppm	average pCO_2 during preindustrial period			
C	CO_2 doublings		$C \equiv \log_2\left(\frac{pCO_2}{pCO_{2,pi}}\right)$			
$\vec{T}$	surface temperature pattern	K	spatial and seasonal pattern of near-surface air temperature			
T	surface temperature	K	global-mean $\vec{T}$			
T_{pi}	preindustrial surface temperature	K	average T during preindustrial period			
ΔT	surface warming	K	$\Delta T \equiv T - T_{pi}$			
ΔT_{eq}	equilibrium warming	K	ΔT after equilibrating to C doublings above preindustrial	linear func. of C	nonlinear func. of C	
ΔT_{2x}	equilibrium climate sensitivity	K	$\Delta T_{2x}(C) \equiv \Delta T_{eq}(C) - \Delta T_{eq}(C-1)$ or $\Delta T_{2x}(C) \equiv \Delta T_{eq}(C)/C$	constant	nonlinear func. of C	
$\vec{T}_{eq}$	equilibrium temperature pattern	K	$\vec{T}$ for a climate in equilibrium			We assume there is a unique $\vec{T}_{eq}$ for each T, so that we can define a function $\vec{T}_{eq}(T)$.
N	net top-of-atmosphere radiative flux	Wm^{-2}	global-mean net top-of-atmosphere radiative flux	linear func. of C and T	quadratic func. of C and T	We assume that $N(C, \vec{T})$ is a function of C and $\vec{T}$, and define $N(C,T) \equiv N(C, \vec{T}_{eq}(T))$
R_f	top-of-atmosphere radiative flux	Wm^{-2}	global-mean top-of-atmosphere radiative flux	linear func. of C and T	quadratic func. of C and T	f can be LW clear, LW cloud, SW, SW surface, SW non cloud atm., or SW cloud
$R_{f,eq}$	equilibrium top-of-atmosphere radiative flux	Wm^{-2}	R_f after equilibrating to C doublings above preindustrial	linear func. of C	quadratic func. of C	See Text S3.
F	radiative forcing	Wm^{-2}	$F(C_0, T_0, \Delta C) \equiv N(C_0 + \Delta C, T_0) - N(C_0, T_0)$	linear func. of C	quadratic func. of C	F is calculated with respect to a background state C_0 and T_0. Usually this is the preindustrial, in which case we define $F(C) \equiv F(0, T_{pi}, C)$.
F_f	radiative forcing component	Wm^{-2}	$F_f(C_0, T_0, \Delta C) \equiv R_f(C_0 + \Delta C, T_0) - R_f(C_0, T_0)$	linear func. of C	quadratic func. of C	See notes for F.
$\tilde{F}$	forcing per doubling	Wm^{-2}	$\tilde{F} \equiv \frac{\partial N}{\partial C}$	constant	linear func. of C	
$\tilde{F}_{pi}$	preindustrial forcing per doubling	Wm^{-2}	$\tilde{F}_{pi} \equiv \frac{\partial N}{\partial C}\Big\rvert_{C_{pi},T_{pi}}$	$\tilde{F} = \tilde{F}_{pi}$	constant	
$\partial_C \tilde{F}$	forcing per doubling CO_2 dependence	Wm^{-2}	$\partial_C \tilde{F} \equiv \frac{\partial^2 N}{\partial C^2}$	0	constant	
λ	radiative feedback	$Wm^{-2}K^{-1}$	$\lambda \equiv \frac{\partial N}{\partial T}$	constant	linear func. of C and T	
λ_{pi}	preindustrial feedback	$Wm^{-2}K^{-1}$	$\lambda_{pi} \equiv \frac{\partial N}{\partial T}\Big\rvert_{C_{pi},T_{pi}}$	$\lambda = \lambda_{pi}$	constant	
$\partial_C \lambda$	feedback CO_2 dependence	$Wm^{-2}K^{-1}$	$\partial_C \tilde{\lambda} \equiv \frac{\partial^2 N}{\partial C \partial T}$	0	constant	$\partial_C \lambda$ can be expressed as $\frac{\partial^2 N}{\partial C \partial T} = \frac{\partial \tilde{F}}{\partial T}$, or the dependence of the forcing per doubling on the temperature of the background state
$\partial_T \lambda$	feedback temperature dependence	$Wm^{-2}K^{-2}$	$\partial_T \lambda \equiv \frac{\partial^2 N}{\partial T^2}$	0	constant	

Text S1. Bootstrapped uncertainty

In order to propagate uncertainty and account for non-normal noise, our confidence intervals are calculated using bootstrapping (Efron, 1979). For the regression-based estimates of $F(C)$, we use a Monte Carlo case resampling approach: instead of using years 1-10 of the T and N time series of a given simulation, we draw from those years 10 times, allowing for duplicates, and regress N against T for that list of years. We repeat this procedure 100,000 times, and use the 2.5% and 97.5% percentiles of the results to estimate the 95% uncertainty band of $F(C)$. For the 21-150 year estimates of $\Delta T_{eq}(C)$, we draw with replacement 130 times before taking the regression, again repeating 100,000 times. Analogous calculations are performed for estimates with different time spans. For the nonlinear factors in Fig. 1c, we recalculate each factor 100,000 times drawing different lists of years for the abrupt2xCO_2 and abrupt4xCO_2/8xCO_2 values.

For uncertainty ellipsoids of λ_{pi} and $\partial_T\lambda$, we reestimate the set of $\{\Delta T_{eq}(C_i), F(C_i)\}$ containing all abrupt2^{C_i}xCO_2 simulations 100,000 times, estimating each $\Delta T_{eq}(C_i)$ and $F(C_i)$ as in the preceding paragraph (for the first four models in Fig. 1a, years 101-1000 are used for $\Delta T_{eq}(C)$, 21-150 for the rest), giving us 100,000 pairs of λ_{pi} and $\partial_T\lambda$. We compute the 75^{th} percentile ellipsoid of the multivariate normal distribution with the mean and covariance of these 100,000 pairs, giving the ellipsoids in Figs. 2 and S6.

2. Equilibrium warming

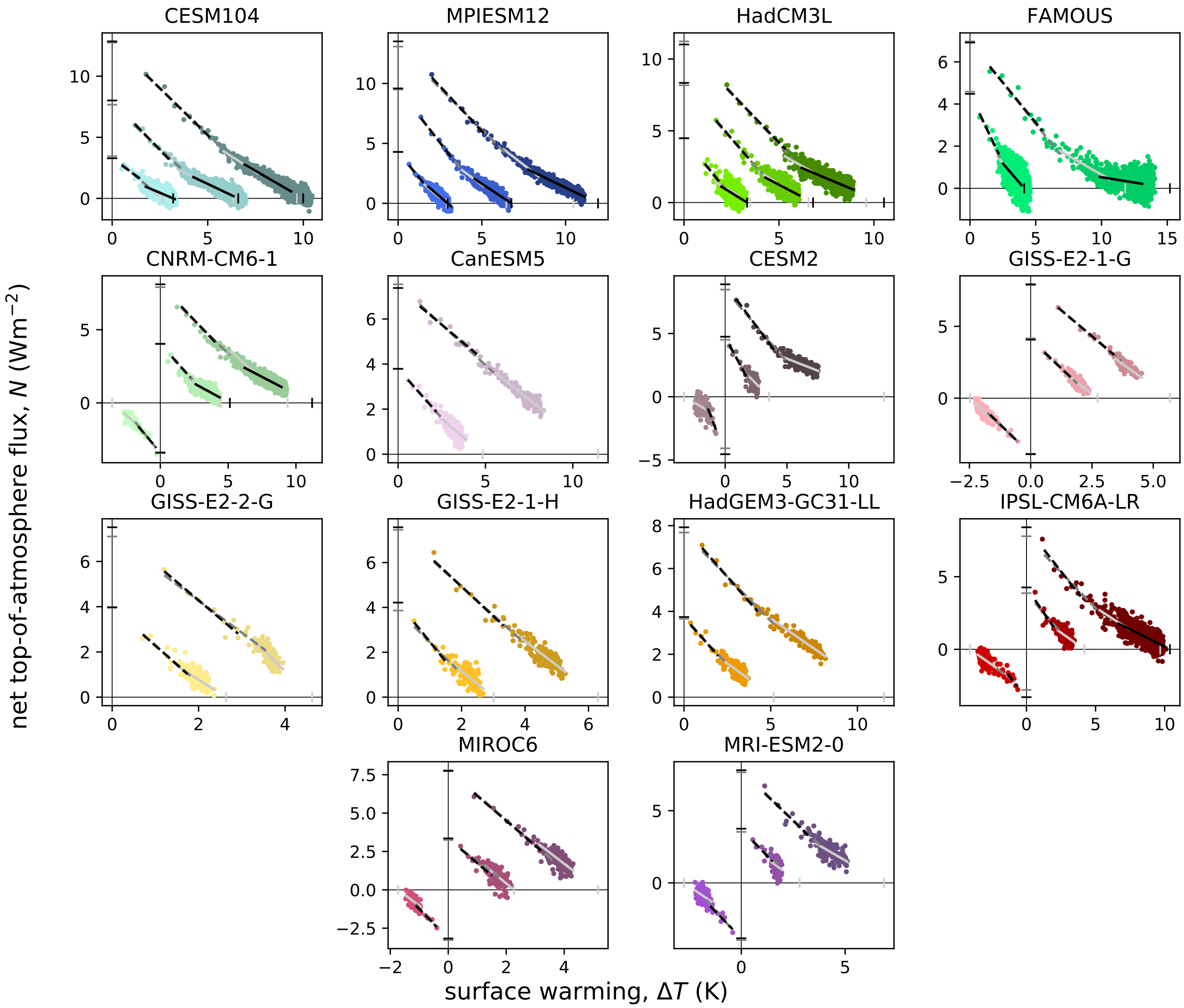

Figure S1. Annual and global-mean averages of net top-of-atmosphere flux (N) vs. surface warming (ΔT) for the simulations shown in Fig. 1. The forcing for each simulation is estimated by regressing years 1-10 of N against ΔT (dashed black lines) and taking the resulting y-intercept (horizontal black ticks). Alternatively, years 1-20 could be used instead (gray dashed lines and horizontal ticks). The equilibrium warming (vertical gray ticks) is estimated as the x-intercept of the regression of N against ΔT over years 21-150 (solid gray lines). For longer simulations, years 101 to n are used for the linear regression (black solid lines and vertical ticks), where n is given in Table S2.

Table S2. Length, in years, of the simulations used in Fig. 1a for each model. For LongRunMIP, only the first 1000 years were used for each model to provide uniformity. For CMIP6/NonLinMIP, only the first 150 years were used unless there were at least 750 years available.

	Model	abrupt0.5x	abrupt2x	abrupt4x	abrupt8x
LongRunMIP	CESM104	-	1000	1000	1000
	MPIESM12	-	1000	1000	1000
	HadCM3L	-	1000	1000	1000
	FAMOUS	-	1000	1000	-
LongRunMIP/NonLinMIP	CNRM-CM6-1	150	750	1000	-
NonLinMIP	CanESM5	-	150	150	-
	CESM2	150	150	150	-
	GISS-E2-1-G	150	150	150	-
	GISS-E2-2-G	-	150	150	-
	GISS-E2-1-H	-	150	150	-
	HadGEM3-GC31-LL	-	150	150	-
	IPSL-CM6A-LR	150	150	900	-
	MIROC6	150	150	150	-
	MRI-ESM2-0	150	150	150	-

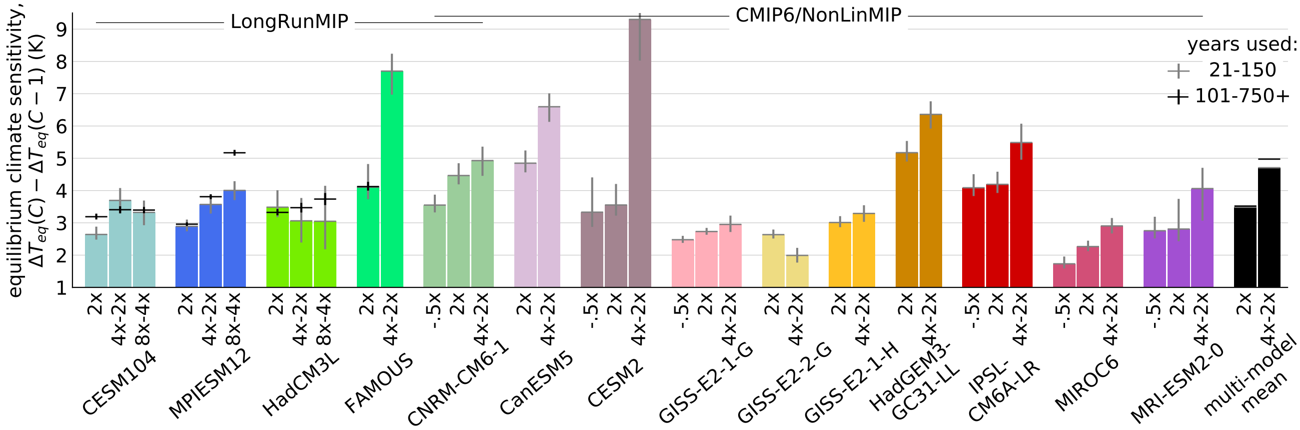

Figure S2. This figure is the same as in Fig. 1a in the paper, except that instead of estimating equilibrium climate sensitivity by dividing equilibrium warming by the number of CO_2 doublings, it is estimated by subtracting estimates of equilibrium warming from successive CO_2 doublings (e.g., the equilibrium climate sensitivity for 4xCO_2 is the equilibrium warming for 4xCO_2 less the equilibrium warming for 2xCO_2). Equilibrium warming is estimated using years 101-1000 for the first four models, and 21-150 for the rest. There are two outliers: 4x for FAMOUS is 11K and 4x for CESM2 is 9.3K. The results are largely the same as in Fig. 1a, except that CESM104 experiences a slight decrease in sensitivity between the 4x and 8x simulations.

3. Radiative forcing

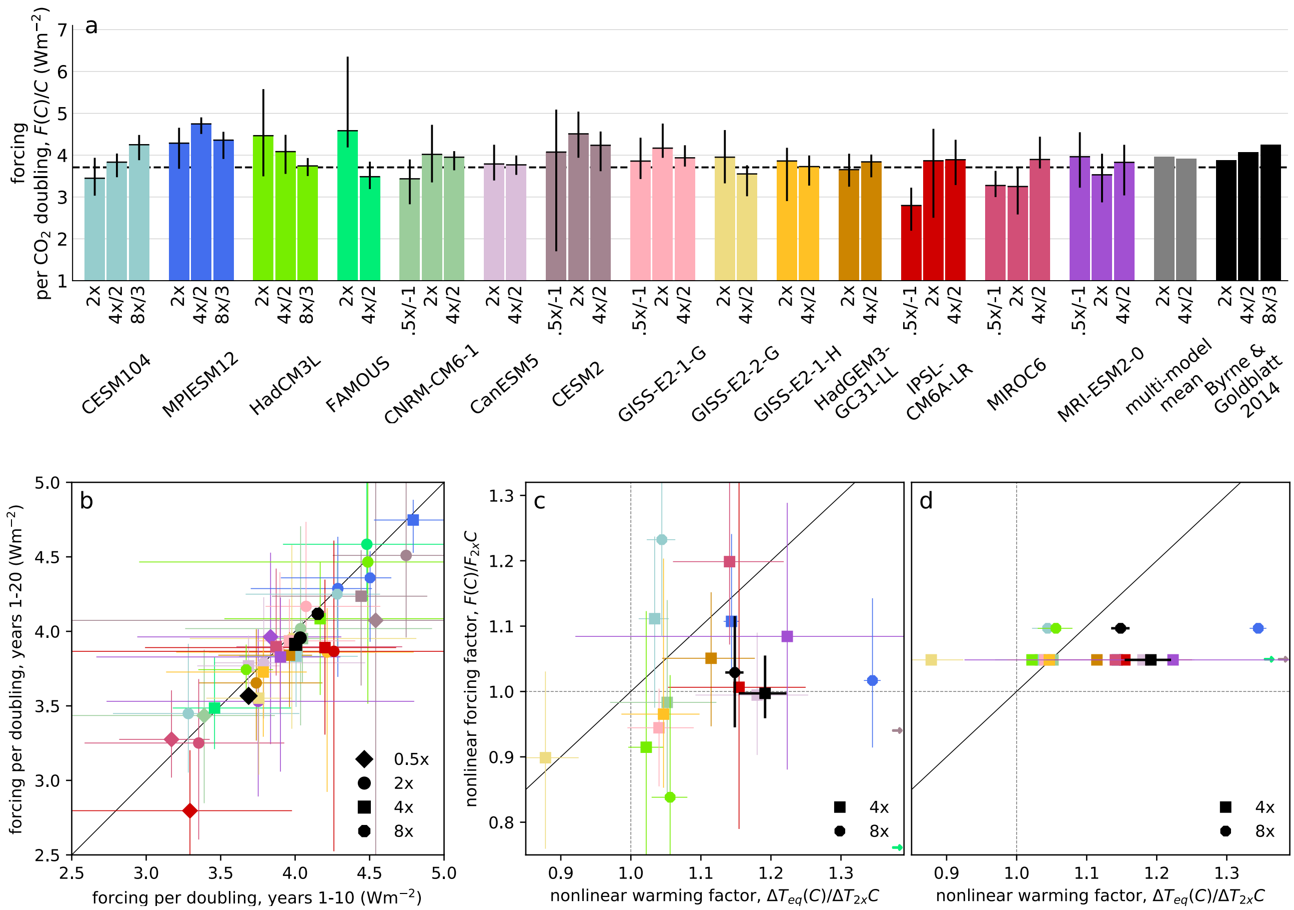

Figure S3. Panel a. mirrors Fig. 1b in the main text, but with estimates of F using years 1-20 instead of 1-10. Panel b. compares these estimates directly, showing that estimates from years 1-20 are biased low (due to the increase in $\partial N/\partial T$ with time, see Fig. S1), but are more certain due to the larger number of years available. Panel c. mirrors Fig. 1c but with the 1-20 year estimates, showing once more that for most models, forcing alone cannot account for the increase in sensitivity. Panel d. is also similar to Fig. 1c, but using the analytic formula of Byrne and Goldblatt (2014), again showing that forcing is insufficient to explain the ECS increase.

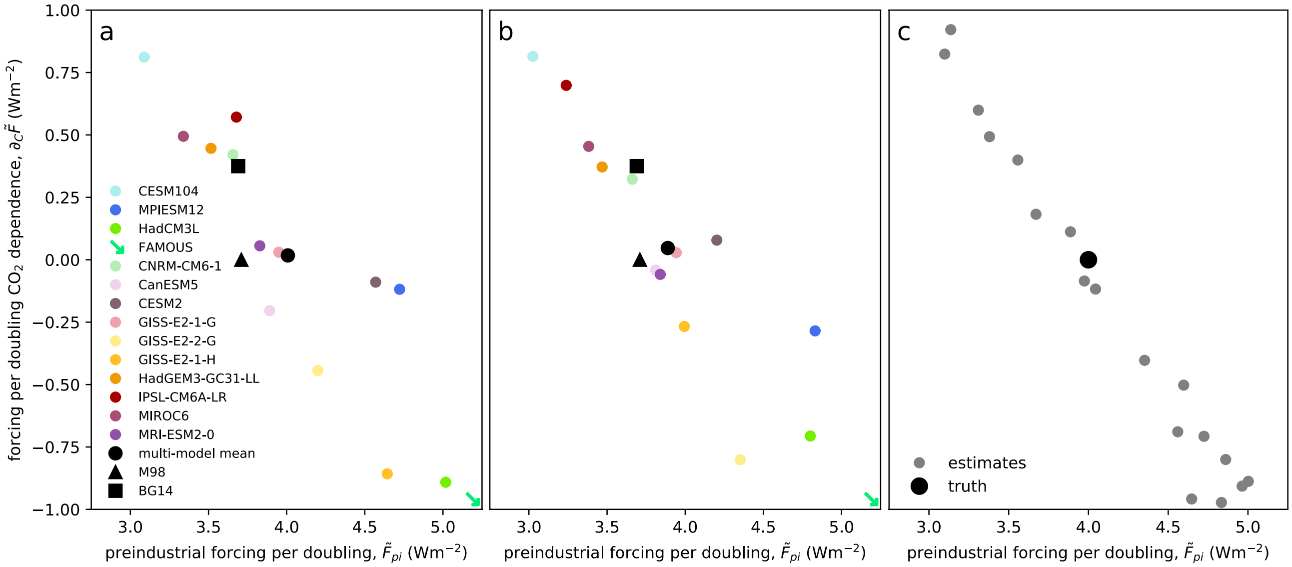

Figure S4. Panels a. and b. show the preindustrial forcing per CO_2 doubling $\tilde{F}_{pi}$ vs. the CO_2 dependence of the forcing per doubling $\partial_C\tilde{F}$ using forcing estimates from years 1-10 and 1-20 respectively (FAMOUS is an outlier, with high $\tilde{F}_{pi}$ and low $\partial_C\tilde{F}$). There is a substantial anticorrelation between the values ($R^2 = 0.77$ for years 1-10, $R^2 = 0.79$ for years 1-20). For both panels, most models have forcing with sublinear dependence on C (i.e., fall to the left of the vertical line at 0), and the multi-model mean is also sublinear, although close to 0. Panel c. shows how this anticorrelation can emerge from the uncertainty associated with regression-based forcing estimates, by plotting twenty draws of a simple model with $\tilde{F}_{pi} = 4$ Wm^{-2}, $\partial_C\tilde{F} = 0$, and a constant $\lambda = -1$ Wm^{-2}K^{-1}, and abrupt2x and abrupt4x simulations with exponential warming (with an e-folding time scale of 5 years) and iid normal noise on N with a σ of 0.4 Wm^{-2}. Estimates of $\tilde{F}_{pi}$ and $\partial_C\tilde{F}$ made using the first twenty years of each pair of simulations are anti-correlated at 95%.

Table S3. Estimates of feedback CO_2 dependence ($\partial_C \lambda$). For details of the forcing estimates, see Text S2.

Model	Forcing estimate	Model used elsewhere in the paper	$n\times CO_2$	F_{cold} (Wm^{-2})	F_{warm} (Wm^{-2})	ΔT (K)	$\partial_C \lambda$ ($Wm^{-2}K^{-1}$)	Reference
CESM1.2.2	regression (1 - 30)	no	2	3.2902	3.6533	7.4085	0.049	Stolpe et al., 2019
CESM2	fixed SST	yes	4	8.8976	8.9759	6.8384	0.0057	original calculation
CNRM-CM6-1	fixed SST	yes	4	7.9909	8.3787	6.0951	0.0318	original calculation
HadGEM2	fixed SST	no	4	6.93	7.10	4.68	0.0182	Forster et al., 2016
HadGEM3-GC31-LL	fixed SST	yes	4	8.0623	8.4026	7.2818	0.0234	original calculation

4. Radiative feedback

Text S2. Estimating feedback CO_2 dependence

Details of the forcing estimates in Table S3 are as follows:

- *CESM1.2.2*: The solar constant is decreased and increased by 25 Wm^{-2}, respectively, and the model is run for several hundred years before branching off abrupt2xCO_2 experiments. The CO_2 forcing is estimated by linearly regressing over the first 30 years of the 2xCO_2 simulations.

- *CESM2, CNRM-CM6-1, & HadGEM3-GC31-LL*: 4xCO_2 forcing is evaluated at pre-industrial conditions (difference between "piSST-4xCO_2" and "piSST" experiments; SST climatology constructed from each models' own control simulation) and at a climate that corresponds to 4xCO_2 conditions (SST and sea ice are taken from years 111-140 of the abrupt4xCO_2 experiments). The forcing in the warmer climate is estimated as the difference between the two experiments "a4SSTice-4xCO_2 and "a4SSTice". The simulations are 30 years long and the first 9 years of the experiments are disregarded, but the results are largely insensitive to this choice. F_{cold} for these two models can also be estimated by the RFMIP (Pincus et al., 2016) "piClim" and "piClim-4xCO_2" experiments for which a common SST climatology is used. The forcing estimates are, however, very similar. For CESM2 it is 8.91 Wm^{-2} and for CNRM-CM6-1 it is 8.00 Wm^{-2} (Smith et al., 2020).

- *HadGEM2*: 4xCO_2 forcing was evaluated twice: with pre-industrial SST, and with SSTs uniformly increased by 4K. This corresponds to a global mean air temperature change of about 4.68 K. This estimate is based on the difference between the "amip4K" and "amip" experiments with the closely related model HadGEM2-A.

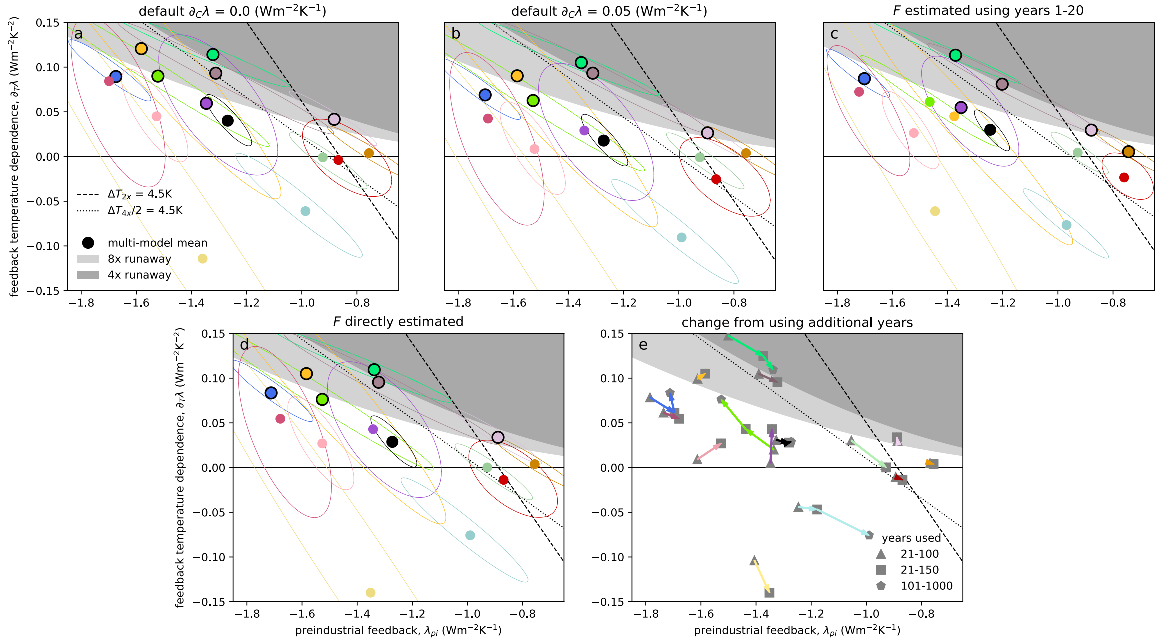

Figure S5. Each panel shows how changing one of our assumptions would affect Fig. 2. In panels a. and b., the default feedback CO_2 dependence $\partial_C\lambda$ is set to 0.0 or 0.05 Wm^{-2}K^{-1} respectively, spanning the values seen in Table S3. While larger (smaller) values of $\partial_C\lambda$ may decrease (increase) our estimates of $\partial_T\lambda$, they also shift the thresholds of nonlinear behavior in parameter space accordingly, so that there is little qualitative effect. Panel c. is like Fig. 2, but with forcing estimates based on years 1-20 instead of 1-10 (note the reduction in uncertainty). Once more, there is little qualitative effect. Panel d. shows the result of using direct estimates of forcing instead of a quadratic fit on the right side of Eq. 8, and panel e. shows the result of using additional years to estimate equilibrium warming. In both cases, results are pretty similar to Fig. 2. For years 101-1000, with the exception of FAMOUS (which the model suggests is in runaway warming), the magnitude of $\partial_T\lambda$ increases, suggesting that the magnitude of the NonLinMIP models' $\partial_T\lambda$ may be biased low.

Table S4. CMIP6 abrupt4xCO_2 simulations with equilibrium warming above 9K (leading to a linear estimate of $\Delta T_{2x} > 4.5$K). All estimates made using publicly available CMIP6 data, except GFDL-CM4, which was made using Winton et al. (2020). Columns give estimates of ΔT_{eq} made using the given number of years.

Model	21 - 150	51 - X	101 - X
ACCESS-CM2	10.71		
ACCESS-ESM1-5	9.63		
CanESM5	11.51		
CESM2	12.85		
CESM2-FV2	13.36		
CESM2-WACCM	11.21		
CESM2-WACCM-FV2	12.09		
CIESM	12.60		
CNRM-CM6-1	9.39	11.02 (X = 1000)	11.19 (X = 1000)
CNRM-ESM2-1	9.25		
E3SM-1-0	11.48		
GFDL-CM4	8.80	10.0 (X = 300)	
HadGEM-GC31-LL	11.49		
HadGEM-GC31-MM	10.80		
IPSL-CM6A-LR	9.56	10.32 (X = 900)	10.34 (X = 900)
KACE-1-0-G	9.88		
NESM3	9.24		
NorESM2-LM	6.01	15.60 (X = 500)	16.65 (X = 500)
TaiESM1	9.33		
UKESM1-0-LL	10.99		

5. Comparing nonlinear terms

Text S3. Estimating the components of the three nonlinear terms

We first create globally and annually averaged time series of the radiative flux, R_f, of each component, f (where f is LW clear-sky, LW cloud, SW, SW surface, SW noncloud atm., and SW cloud), by taking the LW clear-sky, LW cloud radiative effect, and SW all-sky fluxes as output by the models themselves for the first three f respectively, and by calculating the SW surface, SW noncloud atm., and SW cloud using APRP as described in Taylor et al. (2007) for the CMIP6 models (for which we have the necessary variables) for the last three f respectively. We calculate anomalies for each LongRunMIP model by subtracting the average preindustrial value, and for the CMIP6 models by subtracting the linear trend after the branching point.

We define $F_f(C)$ to be the radiative forcing with respect to preindustrial conditions for the component flux f: $F_f(0) \equiv 0$; otherwise we regress years 1-10 of R'_f (defined as above) against ΔT, and extrapolate to find the estimated value of R'_f at $\Delta T = 0$, which is then $F_f(C)$.

We estimate the forcing per doubling CO_2 dependence components by taking the second-order regression of $F_f(C)$ against C, assuming that the regression passes through the origin; that is, we fit the equation

$$F_f(C) = \tilde{F}_{pi,f} C + \frac{1}{2} \partial_C \tilde{F}_f C^2 \tag{1}$$

We estimate the feedback CO_2 dependence components, $\partial_C \lambda_f$, for the five models in Table S3 by finding the components of the "warm" and "cold" forcings estimated in that table (either by regressing time series of the components, or by taking the relevant fluxes from the fixed-SST experiments) and making the same calculation as in Eq. 12 in the text.

In order to ensure that fluxes are calculated with the equilibrium temperature pattern $\vec{T}_{eq}(T)$, we estimate the components of feedback temperature dependence in the following manner. We define $R'_{f,eq}(C)$, the equilibrium anomalous top-of-atmosphere flux for component f at C as follows: $R'_{f,eq}(0) \equiv 0$; for $C \neq 0$, we regress the annually-averaged abrupt2^CxCO_2 time series of the anomaly of the top-of-atmosphere radiative flux f, R'_f (where anomalies are defined as in Section 2) against the time series of ΔT for the same simulation during years 21-150 (for CMIP6 models) or 101-1000 (for LongRunMIP models), and then use this linear fit to extrapolate R'_f to its value at $\Delta T_{eq}(C)$, which is then $R'_{f,eq}(C)$.

We then fit the equation

$$R'_{f,eq}(C) - (\tilde{F}_{pi,f}C + \frac{1}{2}\partial_C \tilde{F}_f C^2) = \lambda_{pi,f}\Delta T_{eq}(C) + \frac{1}{2}\partial_T \lambda_f \Delta T_{eq}(C)^2 + \partial_C \lambda_f C \Delta T_{eq}(C) \quad (2)$$

which is equivalent to Eq. 8 in the main body of the text, except with the $R'_{f,eq}(C)$ term, which is 0 for $N_{eq}(C) = \sum R'_{f,eq}(C)$. For models for which we do not have direct estimates of the feedback CO_2 dependence components, we use the average values of the five models. This gives our estimate of the feedback temperature dependence component $\partial_T \lambda_f$.

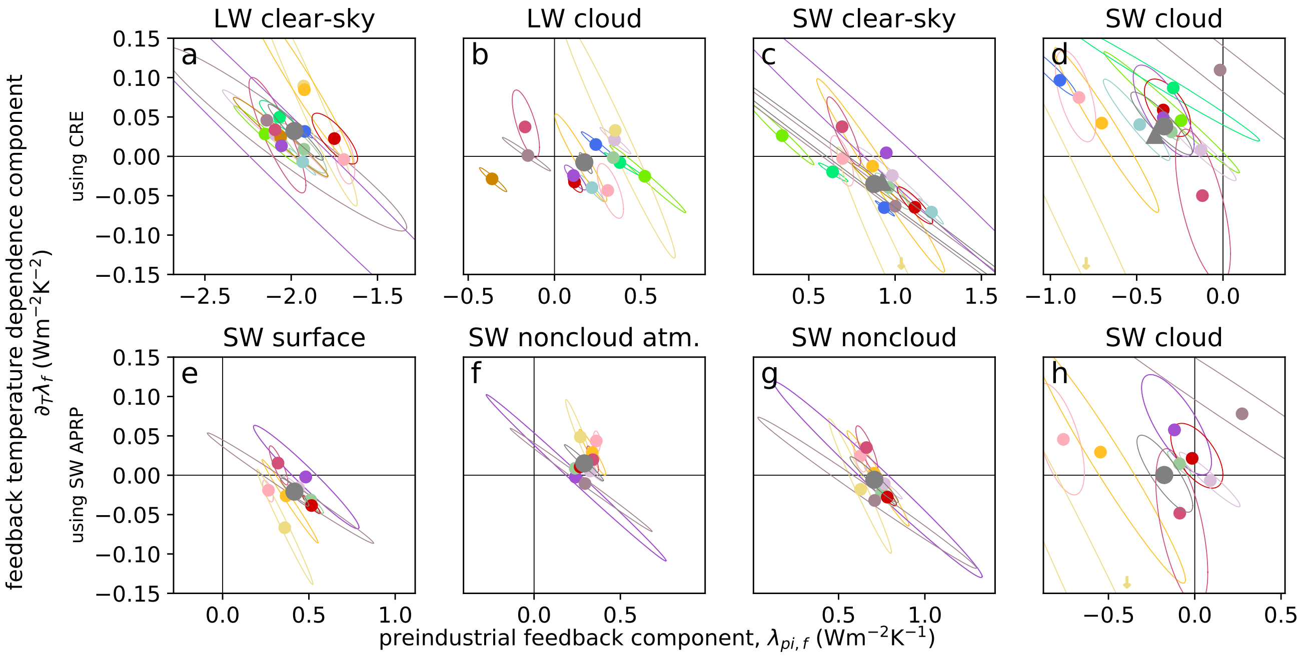

Figure S6. Colored dots in all panels give flux components of preindustrial feedback vs. feedback temperature dependence, and colored ellipsoids give the 75^{th} percentile of uncertainty, where the colors are as in Fig. 1, 2, and 3 in the main body of the paper. Gray dots/ellipsoids give the multi-model mean. Panels a through d give the clear-sky vs. cloud radiative feedback decomposition of the shortwave and longwave feedbacks. Panels e, f, and h give the approximate partial radiative perturbation components for models with the necessary variables available, and panel g is the sum of the values in panels e and f, for comparison with panel c. In panels c and d, the gray triangles give mean values of only the models for which APRP calculations are performed in panels g and h, allowing comparison with the multi-mean values in those panels and an assessment of the bias created by cloud masking, which is present in the top row but not the bottom.

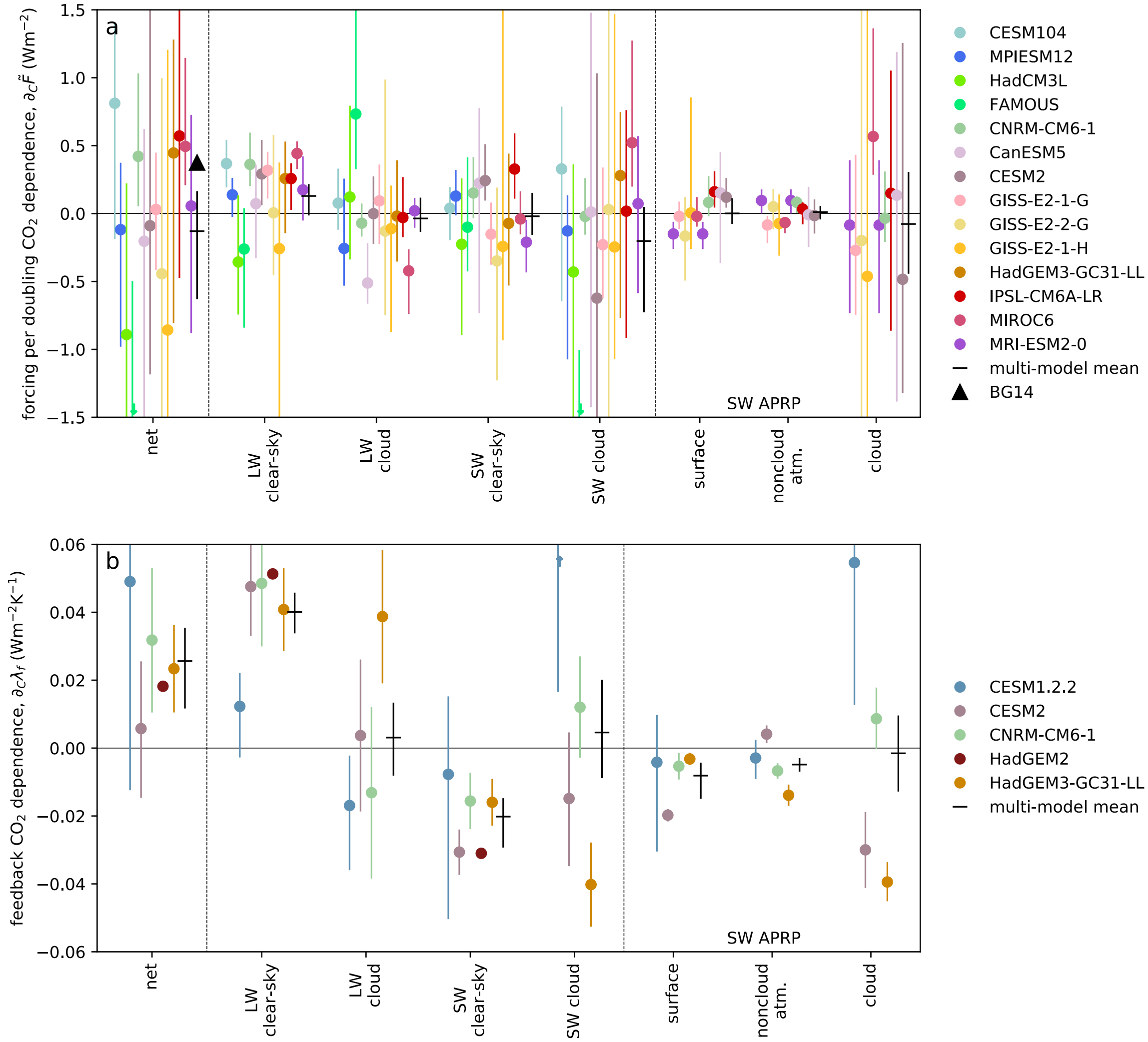

Figure S7. Flux components of the nonlinear terms CO_2 dependence of the forcing per CO_2 doubling ($\partial_C \tilde{F}$, panel a) and feedback CO_2 dependence ($\partial_C \lambda$, panel b); see Text S3 for details. The last three columns of each panel give shortwave approximate partial radiative perturbation components for models with available data. Vertical lines give the 2.5^{th} to 97.5^{th} percentile range of uncertainty. FAMOUS is an outlier for the net and SW cloud nonlinear forcing terms.

References

Byrne, B., & Goldblatt, C. (2014). Radiative forcing at high concentrations of well-mixed greenhouse gases. *Geophysical Research Letters*, *41*(1), 152–160. Retrieved 2019-11-27, from `https://agupubs.onlinelibrary.wiley.com/doi/abs/10.1002/2013GL058456` doi: 10.1002/2013GL058456

Efron, B. (1979). Bootstrap Methods: Another Look at the Jackknife. *The Annals of Statistics*, *7*(1), 1–26. Retrieved 2020-04-23, from `https://www.jstor.org/stable/2958830` (Publisher: Institute of Mathematical Statistics)

Forster, P. M., Richardson, T., Maycock, A. C., Smith, C. J., Samset, B. H., Myhre, G., ... Schulz, M. (2016). Recommendations for diagnosing effective radiative forcing from climate models for CMIP6. *Journal of Geophysical Research: Atmospheres*, *121*(20), 12,460–12,475. Retrieved 2019-12-24, from `https://agupubs.onlinelibrary.wiley.com/doi/abs/10.1002/2016JD025320` doi: 10.1002/2016JD025320

Pincus, R., Forster, P. M., & Stevens, B. (2016, September). The Radiative Forcing Model Intercomparison Project (RFMIP): experimental protocol for CMIP6. *Geoscientific Model Development*, *9*(9), 3447–3460. Retrieved 2020-04-23, from `https://www.geosci-model-dev.net/9/3447/2016/` (Publisher: Copernicus GmbH) doi: https://doi.org/10.5194/gmd-9-3447-2016

Smith, C. J., Kramer, R. J., Myhre, G., Alterskjr, K., Collins, W., Sima, A., ... Forster, P. M. (2020, January). Effective radiative forcing and adjustments in CMIP6 models. *Atmospheric Chemistry and Physics Discussions*, 1–37. Retrieved 2020-04-23, from `https://www.atmos-chem-phys-discuss.net/acp-2019-1212/` (Publisher: Copernicus GmbH) doi: https://

doi.org/10.5194/acp-2019-1212

Stolpe, M. B., Medhaug, I., Beyerle, U., & Knutti, R. (2019). Weak dependence of future global mean warming on the background climate state. *Climate Dynamics*, *53*(7), 5079–5099. Retrieved 2019-11-27, from https://doi.org/10.1007/s00382-019-04849-3 doi: 10.1007/s00382-019-04849-3

Taylor, K. E., Crucifix, M., Braconnot, P., Hewitt, C. D., Doutriaux, C., Broccoli, A. J., ... Webb, M. J. (2007, June). Estimating Shortwave Radiative Forcing and Response in Climate Models. *Journal of Climate*, *20*(11), 2530–2543. Retrieved 2020-03-08, from https://journals.ametsoc.org/doi/10.1175/JCLI4143.1 (Publisher: American Meteorological Society) doi: 10.1175/JCLI4143.1

Winton, M., Adcroft, A., Dunne, J. P., Held, I. M., Shevliakova, E., Zhao, M., ... Zhang, R. (2020). Climate Sensitivity of GFDL's CM4.0. *Journal of Advances in Modeling Earth Systems*, *12*(1), e2019MS001838. Retrieved 2020-04-22, from https://agupubs.onlinelibrary.wiley.com/doi/abs/10.1029/2019MS001838 (_eprint: https://agupubs.onlinelibrary.wiley.com/doi/pdf/10.1029/2019MS001838) doi: 10.1029/2019MS001838